International Journal of Hydrogen Energy 81 (2024) 81–92

Contents lists available at ScienceDirect

International Journal of Hydrogen Energy

journal homepage: www.elsevier.com/locate/he

Feasibility study of LOHC-SOFC systems under dynamic behavior for cargo ships compared to ammonia alternatives

Marco Gambini, Federica Guarnaccia, Michele Manno *, Michela Vellini

University of Rome Tor Vergata, Via del Politecnico, 1, Rome, 00133, Italy

ARTICLE INFO

Keywords:
Hydrogen
LOHC
NEC
Ammonia
Maritime sector
Hard-to-abate

ABSTRACT

Maritime propulsion is recognized as a hard-to-abate sector and its decarbonization will therefore require transversal efforts, including the introduction of alternative fuels to reduce CO_2 emissions. Both ammonia and hydrogen could provide clean power; however, forecasts hint that ammonia will be especially useful for longer routes, while hydrogen suffers from low volumetric energy density. This paper evaluates the feasibility of a cargo ship with a SOFC powertrain equipped with LOHC-based hydrogen storage and compares the sizing and heat management requirements of four LOHC systems, namely N-ethylcarbazole (NEC), dibenzyltoluene (DBT), methylcyclohexane (MCH), decaline (DEC), with an ammonia-based one. The size of the 8.4 MW SOFC system is similar for the five carriers as expected. The dynamic performance of the LOHC system shows that the hydrogen flow rate can be effectively controlled by acting on the LOHC flow rate, reactor temperature, and pressure. However, LOHC systems are heavier (by a factor of 1.6 to 2.1) and larger (by 1.6 to 2.3 times) than ammonia systems. The decalin system results in the lowest mass and volume, while NEC is the heavier, and MCH is the least dense of the evaluated LOHCs. Similarly, the utilization of SOFC waste heat to cover dehydrogenation heat ranges from 45.6 % (NEC) to 27.9 % (ammonia). Overall, even considering the lower reaction temperature, LOHCs do not appear to be competitive with ammonia as hydrogen storage systems in the maritime sector.

1. Introduction

Global shipping emissions in 2018 were responsible for approximately 2.9% of global greenhouse emissions and are projected to increase unless mitigation actions are implemented [1]. CO_2 emissions of large ships (above 5000 tonnage) entering EU ports have been included in the EU Emission Trading System since January 2024, covering 50% to 100% of the voyage emissions, depending on the route. This policy aligns with the revised International Maritime Organization (IMO) greenhouse gas (GHG) strategy, which renewed the net zero GHG emissions goal from international shipping by 2050. Indicative check points for 2030 and 2040 have been introduced and set as emission reduction by at least 20% to 30% and 70% to 80% respectively [2].

The DNV 2021 maritime sector forecast suggested that the future energy mix will likely be made up of different fuels, but many uncertainties remain, so fuel-flexible solutions will be needed to ease the transition [3]. The most promising candidates are ammonia, bio-methanol, bio-LNG, bio-marine gas oil, and synthetic liquefied natural gas. Ammonia is especially considered a promising fuel for the transition to carbon-free energy: blends of ammonia with hydrogen or other gases, ammonia-fired gas turbines [4], and direct ammonia fuel cells [5] could provide useful tools for the energy transition.

Great emphasis has been put on demonstration projects for onboard use of both hydrogen and ammonia and are scheduled for 2025. Liquid hydrogen storage can help raise the otherwise low hydrogen energy density, and may be the best hydrogen storage option for larger vessels. However, high energy demand and long bunkering intervals mean that ships will most likely run on more energy-dense fuels, such as ammonia. In general, hydrogen is expected to perform better for short-sea shipping than deep-sea shipping [6].

Although there are already a small number of hydrogen or hydrogen hybrid ships, more research is key to better tune the characteristics to those of the maritime sector. In fact, already in 1998 Abe et al. predicted a conceptual tanker design for the transport of up to four tanks, each with a volume of 50 000 m^3 for a total power requirement of 100 MW [7]. Throughout the last twenty years, different hydrogen-based maritime projects were carried out, with pressurized hydrogen being chosen as the most common storage solution. The use of liquid hydrogen reduces the volume requirements, but liquefaction, handling,

* Corresponding author.
E-mail addresses: gambini@ing.uniroma2.it (M. Gambini), federica.guarnaccia@students.uniroma2.eu (F. Guarnaccia), michele.manno@uniroma2.it (M. Manno), vellini@ing.uniroma2.it (M. Vellini).

https://doi.org/10.1016/j.ijhydene.2024.07.224
Received 18 June 2024; Received in revised form 10 July 2024; Accepted 15 July 2024
Available online 23 July 2024

storage components cost, lack of infrastructure, and safety issues pose significant limits that must be overcome [8]. The following list includes some examples of hydrogen-powered ships, which are described alongside many others by Kolodziejski [9]:

- The Viking Lady hybrid commercial ship, operated from 2003 to 2018, designed with a 330 kW fuel cell [10].
- The Hydrocat workboat, with diesel engines modified to run on hydrogen with 5% diesel pilot injection. Its success has led to the commissioning of six additional similar models [11].
- The Windcat commissioning service operation vessel will feature a wind turbine and a hydrogen propulsion system and is expected to be operational by 2025 [12]. It will be the first hydrogen-fueled tugboat, with a compressed hydrogen storage capacity of 415 kg [13].
- Edda Breeze, which is a hydrogen-ready commissioning service operation vessel intended to operate with hydrogen stored in Liquid Organic Hydrogen Carriers (LOHCs) [9,14].
- The Energy Observer, a hydrogen-powered self-sufficient ship with two 42 kW electric motors capable of acting as hydro-generators when using wind propulsion during sailing [15,16]. It will be succeeded by the Energy Observer 2 which will run on liquid hydrogen tanks, and will rely on consumption and efficiency optimization to overcome the high volume constraint [9,17].
- The Sea Change ferry featuring 200 kW electric motors with three 120 kW Fuel Cell (FC) stacks, powered by ten 250 bar hydrogen vessels in conjunction with two 50 kWh lithium batteries [18,19].
- The Norwegian MF Hydra launched at the end of March 2023. It is the first liquid-hydrogen FC-powered ferry to operate regularly, although it is a hybrid system that features two 200 kW FCs and two auxiliary biodiesel engines rated 440 kW [9,20]. The success of the project led to the commissioning of two similar ferries expected to operate over much longer distances (100 km). They will rely on hydrogen for at least 85% of consumption and are expected to reduce CO_2 emissions by 26 500 t per year [9,21].

Hydrogen must be produced through electrolysis powered by renewable energies to reduce GHG emissions; however, GHGs would still be emitted and pilot fuel emissions and hydrogen slips must be minimized, with the latter estimated as up to 10% (volume) from production to combustion. Switching from internal combustion engines to fuel cells would remove additional NOx, SOx, and particulate matter emissions. Minutillo et al. focus on the introduction of a small hybrid ferry based on Proton-Exchange Membrane Fuel Cell (PEMFC) technology; different hydrogen storage technologies have been compared, and, regardless of the specific solution, the most critical factors remain the increase in volume and weight [22]. Indeed, the complexity of traditional hydrogen storage introduces additional obstacles: compressed gas features insufficient storage density even at high pressure levels, while liquid hydrogen requires highly insulated tanks and introduces high costs. Liquid organic hydrogen carriers and ammonia could provide cheaper solutions [6]. Indeed, the use of pure hydrogen is critically disadvantaged by its low density: nearly three times lower than that of natural gas, its lower heating value is so low that blending it with natural gas is justified even for stationary applications [23].

Comparing on-board hydrogen storage with compressed hydrogen, liquid hydrogen, or metal hydrides reveals that while PEMFCs lead to up to 60% volume and 56% mass decrease over the traditional diesel engine layout, these hydrogen storage solutions feature significantly lower volumetric and gravimetric energy densities, with an overall reduction in cargo capacity of up to 9% [24]. Perna et al. evaluated the techno-economic feasibility of a solar-driven electrolysis system used to power a fuel cell-based propulsion system for small passenger ferry boats traveling on short routes, revealing that a hydrogen-based system could be competitive, provided that the levelised cost of hydrogen decreases significantly and the value of by-products such as oxygen is suitably recognized [25].

Watanabe et al. provide an interesting overview of the introduction of alternative fuels into the energy mix of the maritime sector for different European countries [26]. Liquid hydrogen is expected to lead to low tank-to-wheel emissions, but leakages and electricity consumption raise the final well-to-wheel impact, which is also highly affected by the future energy mix. In general, while its stage of development is still relatively low, green hydrogen features among most of the prominent studies thanks to the low well-to-wheel carbon emissions [27]. Safety aspects and legal frameworks are still inadequately defined, further affecting the development of the sector [28]: the different properties of hydrogen compared to more conventional fuels imply that safety mechanisms would need to be re-designed [23]. Furthermore, the use of hydrogen from renewable electrolysis still has high production costs and lacks the renewable power source infrastructure [29]; a higher demand could help reduce production costs and lead to greater competitiveness. However, as international ships may purchase fuel in foreign countries, demand uncertainty could have detrimental effects on national hydrogen prices [30].

LOHCs are organic compounds that can undergo reversible hydrogenation and dehydrogenation reactions [31]. Through the saturation of double C–C bonds, hydrogen is stored exothermically in the carrier molecules; similarly, endothermic dehydrogenation occurs as those bonds are desaturated. LOHCs meet important goals for ideal hydrogen storage and use, including: relatively high energy density, high safety and easy handling, high purity outflow with low to no losses, and the possibility of using existing pipeline infrastructure [32,33]. LOHCs may not be attractive for small-scale applications in the transport sector; however, for long-distance, large-scale transportation, including the maritime sector, LOHCs could outperform other storage solutions [34]. Furthermore, LOHC-based storage systems have also been experimentally reported to be able to deal with significant variations in power demand by tuning the thermodynamic operating conditions and the LOHC flow rate [35,36].

Aakko-Saksa et al. consider the propulsion of a 41 MW ship as a possible LOHC application [37], with a one-tank system capable of handling loaded and unloaded LOHC to reduce the volume of the system. Niermann et al. carried out a comprehensive techno-economic analysis and comparison of the main LOHCs, finding that the most promising ones are dibenzyltoluene (DBT) for energy transport and storage applications and N-ethylcarbazole (NEC) for mobility applications [32]. For mobile applications, storage capacity and energy density have to be considered due to the direct effect on the system size and weight. Additional parameters are dehydrogenation temperature (assuming PEMFC coupling), cold start time and dynamic behavior.

Reaction heat to drive hydrogen release is a major challenge for LOHC systems. In the operating temperature range, methyl-cyclohexane (MCH) shows a negligible effect of pressure on the energy balance; however, it is recommended for the thermochemical recovery system to set the LOHC pressure in the 1.5 bar to 2.0 bar range [38]. Spatolisano et al. investigated the techno-economic aspects of hydrogen transport through LOHCs; dehydrogenation was found to be the property that most affects system costs [39]. The dehydrogenation process of a charged LOHC draws considerable heat and provides a major drawback of LOHC systems.

Switching from PEMFCs to Solid Oxyde Fuel Cells (SOFCs) gives access to higher electrical efficiency (about 50%) and fuel flexibility [40], and could provide the dehydrogenation heat requirement through waste heat recovery [41]. Significant insights into the LOHC-SOFC coupling in DBT systems have been provided in the literature [42,43]. The system layout was described with respect to its transient operating behavior; its electrical efficiency was about 45% allowing for optimal heat integration without exceeding thermal limits. Different operating phases have been analyzed in detail with a focus on system warm-up. A specific protocol was designed to avoid damaging the SOFC [43]. It was demonstrated that LOHC vapor should not harm the

operational stability of the stack: at high temperature all the components of the LOHC vapor are converted to methane through catalytic hydrocracking and reforming processes. Methane is then consumed in the fuel cell together with the hydrogen fuel [42].

Traditional powertrains rely on diesel engines, with about 50% of the total fuel energy turning into mostly low-temperature waste heat: the low heat quality makes heat recovery quite challenging [44]. Heat recovery is in some way easier in SOFC-based powertrains since heat is available at high temperature. Micoli et al. simulate a 12 MW SOFC system powered by liquefied natural gas (LNG) set to provide both electricity and part of the thermal energy demand: by maximizing steam production, about half the thermal energy demand is covered by the waste heat, returning an approximate LNG saving of 14.4% [45]. SOFC waste heat recovery holds indeed a huge potential for the maritime sector. Ouyang et al. proposed and simulated a combined cooling, cascaded SOFC power and desalination system; the system efficiency improves significantly when compared to the reference SOFC layout, and could even effectively satisfy the crew's daily needs of cold energy and fresh water [46].

This paper provides insight into the possible application of LOHC carriers in the maritime sector. More specifically, a LOHC-SOFC system is sized using a realistic load scenario taken from Di Micco et al. [47]. The results of the sizing process are reported for different carriers, namely: dibenzyl toluene (H0-DBT) - perhydro-dibenzyl toluene (H18-DBT), N-ethylcarbazole (H0-NEC) - perhydro-N-ethylcarbazole (H12-NEC), napthalene (H0-NAP) - decalin (H10-DEC), and toluene (H0-TOL) - methylcyclohexane (H6-MCH). The dynamic response of the system is evaluated through a *Matlab-Simulink* model, making use of a multi-parameter control strategy to meet the hydrogen demand. Simulation results are reported for NEC systems with a Pt/C 5 wt.% catalyst [48], but the proposed method could be used to simulate any other carrier by changing the specific kinetic properties. However, it is worth observing that while gravimetric performances are intrinsically associated with the carrier molecule, different catalysts would result in different operating conditions, kinetic properties and, possibly, dynamic response. The sizing results are then compared with the ammonia-based system available in the literature [47] to evaluate the potential of LOHC storage as a technology that can contribute to the decarbonization of the maritime sector; the different solutions are compared with respect to the volume, mass and heat requirements. The structure of this paper follows its purpose and is consequently subdivided into the Methods and Results sections, each with three subsections to cover the SOFC and LOHC design and the dynamic performance. The load profile used for the simulation is presented in the Methods section.

2. Methods

For the proposed system layout, the preliminary sizing comprises two consecutive steps: first, the SOFC is sized, then the LOHC system. While the preliminary design of the SOFC requires only the load profile, the size of the LOHC system also depends on the conversion efficiency. The dynamic behavior of the system is then simulated to assess whether the power demand can be met. To meet the power demand, three control strategies are implemented, based on the LOHC mass flow rate, reactor temperature, and reactor pressure. The waste heat from the SOFC is recovered to meet the heat demand of the LOHC subsystem.

The power demand is taken from Di Micco et al., which present the design, modeling, and feasibility assessment of two ammonia-based fuel cell powertrains (a PEMFC and a SOFC system) for a container ship [47]. The authors provide a comparison with respect to a conventional diesel layout with emphasis on the reduction in cargo due to the additional weight (and volume) introduced by the ammonia system, as well as on the need to recognize the value of the avoided CO_2. The mass and volume of the fuel storage are taken as reference for LOHC systems, while the economic aspects of the analysis are beyond the scope of this

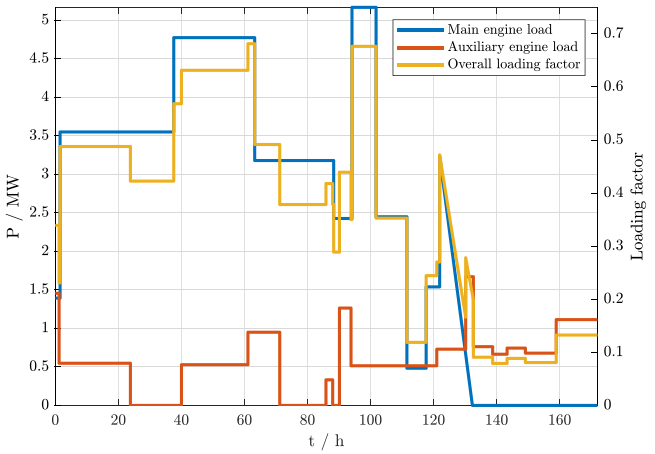

Fig. 1. Simplified main and auxiliary engines power demand, and corresponding overall load factor for a unified conversion system with a rated power of 8.4 MW. The main engine and the total load have the same power rating, while the auxiliary engine has a rated power of 3.5 MW.

article. In the same way, broader considerations regarding production and transportation, as well as environmental impact, could be analyzed through Life Cycle Assessment (LCA) tools; however, the aim of this article is to evaluate the ability of LOHC systems to follow a typical maritime load, and to discuss how these systems compare to the more widely recognized ammonia systems in terms of footprint and mass.

Finally, for the purposes of this analysis, the actual methods of heat recovery are not evaluated. The ability to reuse waste heat is assessed based on the reaction temperature and the heat required for dehydrogenation. Effective integration of heat recovery requires a more specific and detailed analysis; both LOHC and ammonia systems require high-temperature heat recovery to drive hydrogen release without excessively penalizing electrical efficiency. Using heat to drive dehydrogenation reduces the heat available for other potential applications and could negatively impact the overall system efficiency. Similarly, for the comparison between ammonia and LOHC, the size and weight of the systems are calculated in a simplified manner, considering only the carriers. Reactors, storage tanks, pumping systems, possible filtration systems, and auxiliaries introduce additional encumbrance. The two chains present many similarities and have therefore been omitted from the analysis; however, a comparison with traditional systems would require a more detailed characterization.

2.1. Load profile

Di Micco et al. provide the load profile over time of the main and auxiliary engines of a container ship with 11 271 t of dead weight tonnage and cruise duration of 172 h at an average speed of 18.5 knots; the rating power of the engines is 8.4 MW and 3.5 MW, respectively [47]. The two demands can be combined, and since the overall power demand is below the power rating of the main engine, they can be satisfied by a single fuel cell stack.

The load profiles assumed for the purpose of this paper have been smoothed to filter out low-scale fluctuations, and are presented in Fig. 1, also in terms of the load factor (ratio of instantaneous power demand to rated power). Auxiliary and main engine load profiles shift, and their relative magnitude leads to a final demand that is, most of the time, below the reference threshold of 65% [47,49]. This value is associated with the oversizing required to face adverse weather conditions, which would increase the load factor associated with navigation.

2.2. SOFC design

Given the power demand that the SOFC stack must meet, its polarization curve returns the associated efficiency for a given load factor. More specifically, the SOFC efficiency is evaluated as in Eq. (1):

$$\eta_{stack} = \frac{V_{stack} I}{\dot{m}_{\mathrm{H_2}} \mathrm{HHV}} \tag{1}$$

as the ratio of the electrical power output that depends on the stack current I and voltage V_{stack} to inlet rate of chemical energy consumed, given by the product of hydrogen mass flow rate $\dot{m}_{\mathrm{H_2}}$ and Higher Heating Value (HHV).

The stack current is associated to the inlet mass flow rate of hydrogen for a set fuel utilization factor U_f and number of cells in the stack:

$$\dot{m}_{\mathrm{H_2}} = M n_{cells} \frac{I}{zFU_f} \tag{2}$$

with M being the molar mass of hydrogen, $z = 2$ the number of electrons involved in the reaction, and F the Faraday constant.

The stack voltage, assuming homogeneous conditions, depends on the cell voltage as follows:

$$V_{stack} = n_{cells} V_{cell} \tag{3}$$

and the cell voltage for a given current density is returned by the SOFC polarization curve. In this paper, a SOFC model developed and validated by Hafsia et al. [50] and Ranjbar et al. [51] is used to calculate the polarization curve, which gives the cell voltage, Eq. (5), as the difference between the reversible (Nernst) voltage, Eq. (4), and the activation, ohmic and concentration overvoltages, Eq. (6).

$$V_{rev} = V^0(T,p) - \frac{RT}{2F} \log \frac{p_{\mathrm{H_2O}}}{p_{\mathrm{H_2}} p_{\mathrm{O_2}}^{0.5}} \tag{4}$$

$$V_{cell} = V_{rev} - V_{loss} \tag{5}$$

$$V_{loss} = V_{act} + V_{ohm} + V_{con} \tag{6}$$

The overvoltages depend on the activation overpotential (anode, cathode), the ohmic overpotential (anode, cathode, electrolyte), and the concentration overpotential term (anode, cathode). Those terms are subtracted from the reversible voltage evaluated for the cell operating conditions (pressure, temperature, chemical potential of reactants).

The electric conductivity (σ) of electrolyte, cathode, and anode can be evaluated with Eq. (7), with the following values of the parameters: $\sigma_0 = 3.34 \times 10^4\,\Omega^{-1}\,\mathrm{cm}^{-1}$, $b = 10\,300\,\mathrm{K}$ for the electrolyte; $\sigma_0 = 4.2 \times 10^7\,\Omega^{-1}\,\mathrm{cm}^{-1}$, $b = 1200\,\mathrm{K}$ for the cathode; $\sigma_0 = 9.5 \times 10^7\,\Omega^{-1}\,\mathrm{cm}^{-1}$, $b = 1150\,\mathrm{K}$ for the anode [51].

$$\sigma_i = \sigma_{0,i} \exp \frac{-b_i}{T} \tag{7}$$

These values are used to evaluate the ohmic overpotential for each component accounting for the layer thickness (δ) and the SOFC current density ($j = I/A_{cell}$), as seen in Eq. (8). Overpotential values are here reported in $\mathrm{V\,m^{-2}}$; absolute values are obtained replacing the current density (j) with the current value.

$$V_{ohm} = \sum_i \frac{\delta_i}{\sigma_i} \cdot j \tag{8}$$

Activation losess at the electrode-electrolyte interface introduce a further loss mechanism. The exchange currents in the cathode and anode (j_0) are evaluated with respect to activation energy (E_a), an exponential factor (γ) and temperature as in Eq. (9):

$$j_{0,i} = \gamma_i \frac{RT}{2F} \exp\left(-\frac{E_{a,i}}{RT}\right) \tag{9}$$

The resulting overpotential is expressed by Eq. (10) with the arsinh method.

$$V_{act} = \sum_i \frac{RT}{F} \operatorname{arsinh}\left(\frac{j}{2j_{0,i}}\right) \tag{10}$$

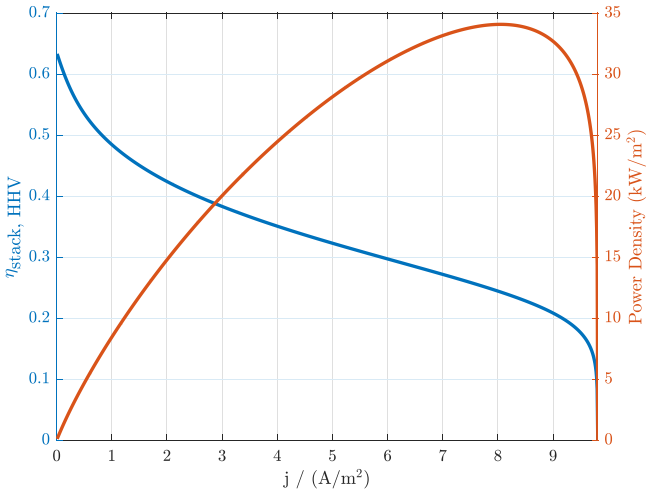

Fig. 2. SOFC derived power density (left y-axis), and corresponding stack efficiency over the HHV (right y-axis).

Concentration overpotential is due to concentration of the reactants at the Triple Phase Boundary (TPB) being different than in the bulk, so it is related to a mass diffusion-limited regime. For the cathode and anode regions Eqs. (11) and (12) are applied.

$$V_{con,c} = \frac{RT}{4F} \log \frac{p_{\mathrm{O_2}}}{p_{\mathrm{O_2},TPB}} \tag{11}$$

$$V_{con,a} = \frac{RT}{2F} \log \frac{p_{\mathrm{H_2}} p_{\mathrm{H_2O},TPB}}{p_{\mathrm{H_2},TPB} p_{\mathrm{H_2O}}} \tag{12}$$

Eqs. (13)–(15) are used to evaluate partial pressures, with D_{eff} being the effective diffusion coefficient [52].

$$p_{\mathrm{O_2},TPB} = p - (p - p_{\mathrm{O_2}}) \exp \frac{jRT\delta_c}{4FD_{eff,c}p} \tag{13}$$

$$p_{\mathrm{H_2},TPB} = p_{\mathrm{H_2}} - \frac{jRT\delta_a}{2FD_{eff,a}p} \tag{14}$$

$$p_{\mathrm{H_2O},TPB} = p_{\mathrm{H_2O}} + \frac{jRT\delta_a}{2FD_{eff,a}p} \tag{15}$$

The required cell area A_{cell} is evaluated by assuming the maximum power density for the design point corresponding to the rated power output. As a consequence, due to the shape of the polarization curve, the stack efficiency at partial load is always higher than at the design point.

The parameters required by the SOFC sizing model are summed up in Table 1. The resulting stack polarization curve is represented in Fig. 2, which also shows the stack power density.

2.3. LOHC system design

The sizing of the SOFC stack allows to associate the stack efficiency to each load conditions. The effective chemical energy $E_{\mathrm{H_2}}$ required to satisfy the power demand is defined in Eq. (16) as the integral of the power demand divided by the SOFC efficiency; the average SOFC efficiency is thus given by Eq. (17).

$$E_{\mathrm{H_2}} = \int_0^T \frac{P(t)}{\eta(t)} dt \tag{16}$$

$$\bar{\eta} = \frac{1}{E_{\mathrm{H_2}}} \int_0^T P(t) dt \tag{17}$$

The hydrogen mass, Eq. (18), that must be stored is obviously derived from the total energy requires; the corresponding mass of LOHC m_{LOHC}, Eq. (19), is a function of the LOHC maximum gravimetric

Table 1
SOFC modeling parameters [50,51]. C., A. and E. abbreviations stand for cathode, anode and electrolyte.

Variable	Value	Variable	Value
Effective diffusivity (C.)	5×10^{-6} m^2 s^{-1}	Effective diffusivity (A.)	2×10^{-5} m^2 s^{-1}
Exponential factor (C.)	2.35×10^{11} A m^{-2}	Exponential factor (A.)	6.54×10^{11} A m^{-2}
Activation energy (C.)	137 103 J mol^{-1}	Activation energy (A.)	140 103 J mol^{-1}
Thickness (C.)	50 µm	Thickness (A.)	500 µm
Thickness (E.)	10 µm	H_2 HHV	141.8 MJ kg^{-1}

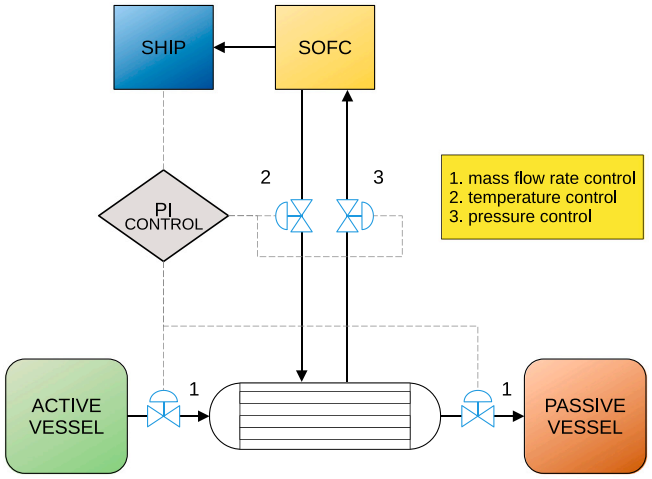

Fig. 3. LOHC sub-system layout: a plug flow reactor is coupled with two vessels allowing for multiple reactor passages. Three control strategies are considered: reactor pressure and temperature, and LOHC mass flow rate.

energy density (w) and the maximum acceptable change in the Degree of Hydrogenation (DOH), which depends on its lower and upper boundary.

$$m_{H_2} = E_{H_2}/\mathrm{HHV} \tag{18}$$

$$m_{LOHC} = \frac{m_{H_2}}{w\left(\mathrm{DoH}_{max} - \mathrm{DoH}_{min}\right)} \tag{19}$$

The corresponding volume can then be evaluated and used to initialize the reactor design. Fig. 3 provides a brief description of the system layout; its configuration, operating characteristics and preliminary sizing procedure described in detail in a previous paper by the authors [53].

The system includes a plug flow reactor whose filling level may vary throughout the operation. At the design point, half the section is assumed empty [42], and the flow direction alternates going from one vessel (active) to the other (passive), allowing for multiple reactor passages. This design reduces the required reactor length without compromising on the reactor residence time and enables further control over the reaction. While the amount of loaded LOHC stored is associated with the energy content of the system, the power demand determines the LOHC flow rate in the reactor. By changing the LOHC volume distribution between the reactor and the vessels through the parameter f_r, defined in Eq. (20), the energy-to-power ratio E_{H_2}/P can be changed to better match the system requirements. Control strategies are further described in Section 2.4.

$$f_r = V_{reactor}/V_{tot} \tag{20}$$

The heat demand of the dehydrogenation process, which is mostly due to the reaction enthalpy, is supplied by a fraction of the SOFC waste heat. NEC thermophysical properties have been evaluated using a group contribution approach validated, whenever available, against data available in the literature [54], while kinetic parameters were defined using experimental data [48,55]. DEC and MCH properties were taken from the PubChem database [56] while DBT data were extracted from the cited HySTOC report [57]. Dehydrogenation enthalpy was taken from the literature [58].

2.4. Control strategies

As illustrated in Fig. 3, multiple control strategies are put in place to meet user demand. Both temperature and pressure control have already been proposed in previous articles by the authors [53,59,60]. As hydrogen release is ruled by kinetic rates in the form of Eq. (21), either variable can be changed to either fasten or slow the hydrogen release. More specifically, in the case of NEC, the kinetic rate can be modeled with reasonable accuracy with Eq. (22) [31]. The kinetic parameters required by this kinetic model are discussed in previous articles [53,60] and are summarized in Table 2. Finally, the hydrogen flow rate is proportional to the product of the LOHC mass flow rate in the reactor and the kinetic rate, as shown by Eq. (23), which ultimately highlights how the three control variables identified in Fig. 3 affect the system output.

$$r = -\frac{\mathrm{dDoH}}{\mathrm{d}t} = k_0 \cdot f(T) \cdot g(p) \cdot \mathrm{DoH}^n \tag{21}$$

$$r = k_0 \exp\left(-\frac{E_a}{RT}\right) \exp\left(-bp\right) \mathrm{DoH}^2 \tag{22}$$

$$\dot{m}_{H_2} = w\, \dot{m}_{LOHC}\, r\,(T, p, \mathrm{DoH}) \tag{23}$$

Thus, for a given catalyst (k_0), it is possible to increase the hydrogen output with an increase in LOHC flow rate, an increase in reactor temperature, or a decrease in pressure. All three control strategies are executed through individual Proportional–Integral (PI) controllers reacting to the error between the actual hydrogen release and the target release determined by the instantaneous power demand. In the proposed layout, the primary control parameter is the LOHC flow rate, with temperature and pressure acting as secondary and tertiary control parameters. The hierarchical order of action is enforced by inserting time delays over both the temperature and pressure controllers, delayed, respectively, by one and two simulation steps; this hierarchy is further reinforced by the proportional gain values, which are summarized in Table 3, together with the integral gains and the lower and upper bounds for each control variable. Temperature and pressure limits have been discussed in a previous paper [53] but actual controller gains have been changed to allow for stable operation in this new parallel control setup. The LOHC flow rate is assumed to be controlled through the opening ratio of the valves connecting the active vessel to the reactor (Fig. 3): throughout the operation it can be changed from zero to double the design value. The valve is further subjected to an additional check to avoid reactor overfilling (i.e., LOHC volume greater than the reactor volume).

Despite the number of control strategies deployed, small errors between hydrogen release and demand can be observed during transient operation. Introducing a small hydrogen buffer may improve the system response during these transients; the buffer level would rise as the instantaneous error is positive, while the vessel empties when the actual release does not meet the demand. If the cumulative integral of the error is negative, the amount of hydrogen released by the system up to a given time instant is less than the amount needed to meet the demand. Otherwise, if the integral is always positive, the introduction of the hydrogen buffer would enable both higher autonomy and better usage of the energy storage; however, the overall volume and weight

Table 2
Parameters required by the kinetic model.

Variable	Value	Source	Variable	Value	Source
Activation energy E_a	121 kJ mol^{-1}	[31]	Reaction enthalpy ΔH_r	50.6 kJ mol$^{-1}_{H_2}$	[61]
Pressure coefficient b	1.397 bar^{-1}	[31]	Frequency factor k_0	2.609×10^{12} min^{-1}	[31]

Table 3
Controlled variables upper and lower bounds, and PI controllers proportional and integral gains. Controllers operate in parallel over the hydrogen release error. Mass flow rate control bounds are set with respect to the nominal inlet LOHC mass flow rate.

Variable	Lower bound	Upper bound	Proportional gain	Integral gain
Temperature	433.15 K	500.15 K	20.00	2.00
Pressure	1.1 bar	5 bar	2.00	0.20
LOHC flow rate	0%	200%	10.0	0.01

of the LOHC subsystem would increase. Although the hydrogen buffer component is not modeled in this analysis, the cumulative error between the actual and target flow rate cumulative integral is evaluated to assess the effectiveness of the control system.

3. Results and discussion

Results are presented below following the order of presentation proposed in Section 2, distinguishing between the sizing sections (SOFC and LOHC systems) and the dynamic response. While the first section regarding the SOFC is not influenced by the choice of hydrogen carrier, the second section shows the sizing results obtained with the choice of NEC, DBT, DEC, or MCH as hydrogen carriers, and compares them to the results available in the literature related to ammonia [47]. The dynamic response of the NEC system is finally analyzed to test the technical feasibility of LOHC systems to follow a dynamic load. Although sizing of the LOHC system is required to proceed with the dynamic simulation, this provides crucial information about the feasibility of a LOHC-based storage system. Therefore, the load response subsection is presented just after the SOFC design, while the LOHC system design and the comparison with ammonia-based systems are presented at the end of this section.

3.1. SOFC design

Table 4 summarizes the main characteristics of the SOFC stack sizing.

The stack surface has been calculated by choosing the maximum power density (see Fig. 2) as the rated operating conditions (load factor equal to one). Fig. 4 represents the efficiency profile for the sized stack with respect to the load factor. The operating conditions resulting from the load have been identified through the corresponding load factors (see Fig. 1) and highlighted as red dots.

The model returns an average efficiency (47%) in agreement with the results presented by Di Micco et al.[1] in the paper taken as Ref. [47]. Given the gravimetric and volumetric power density, provided in the reference paper, of 18.4 kW t^{-1} and 10.1 kW m^{-2} respectively, the resulting SOFC mass and volume are as featured in Table 4. The values reported by [47] are associated with a peak power of 8.3 MW instead of the nominal 8.4 MW, but otherwise perfectly align.

Table 4 also provides the efficiency range associated with the lowest and highest power demand for the given stack, corresponding respectively to the highest (57.2%) and lowest (36.0%) efficiency (HHV-based), while the average efficiency is 41.28%. Dividing the energy

[1] The value reported in the reference is 57% (LHV). However, using the provided data to evaluate the average load factor reveals that it must be instead 47%.

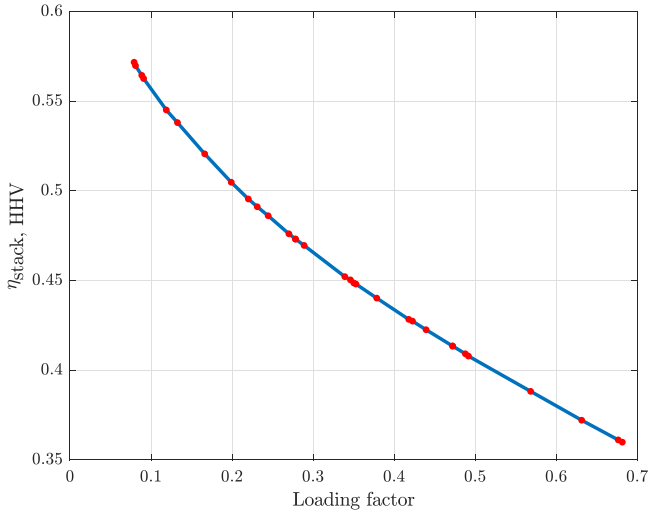

Fig. 4. SOFC loading curve for $T = 750$ °C and $p = 1.1$ bar, as in [47]. Red dots indicate the load factors of Fig. 1.

requirement by the hydrogen heating value returns the minimum hydrogen mass required onboard. The current density range is reported as well and is associated with an overall stack voltage of 480 V as proposed by Di Micco et al.. The associated voltage and current density values are also reported.

In general, the ammonia and LOHC propulsion systems are very similar, as should be expected. However, it must be noted that in the future ammonia-powered ships could possibly rely on alternative, more compact solutions such as ammonia-fueled engines or direct ammonia fuel cells [62,63].

3.2. Dynamic load

The hydrogen carrier chosen to test the dynamic response is NEC. Table 5 lists the initial conditions assumed for the dynamic simulation and the range of DoH values allowed during operation.

Fig. 5 depicts the effective hydrogen release over time, compared to the hydrogen mass flow rate demand that has been evaluated coupling data from Figs. 1 and 4. The LOHC system is flexible enough to cover the demand throughout the entire operating time. Despite the high variability of the load, delay time and overshooting are limited in duration and intensity. Switching to more realistic ramp-like load modulation would reduce the associated misalignment, as highlighted by the ramp transition zoom panel.

Fig. 6 provides the trend for each control parameters that led to the presented release profile. Analysis of the profiles reveals that the inlet mass flow rate is mostly relatively close to the design value (100% in the top panel), with fast increases or decreases corresponding to the step transition in Fig. 1. Similarly, after the initial temperature drop and pressure increase, both profiles follow more variable trends. As a hierarchical action order has been introduced through time delays, fast variations associated with load step changes are followed primarily by the LOHC flow rate, with temperature and pressure control modulating the discharge to compensate for the decreasing DoH value over time. The two profiles are quite similar due to both being associated with hydrogen discharge through an exponential factor [31], although pressure has to increase to hinder the reaction, while the opposite is true

Table 4
SOFC stack sizing and main features. [47] stack are reported to ease the comparison.

Variable	Value	Variable	Value
Surface	232.43 m^2	Volume	831.68 m^3
Mass	456.52 t	Current density range	0.27 A cm^{-2} to 3.7 A cm^{-2}
Average efficiency	41.28% (HHV)	Average efficiency	48.38% (LHV)
Efficiency range	35.99% to 57.17% (HHV)	Average load factor	0.37
Current density efficiency range	0.27 A cm^{-2} to 41.28 A cm^{-2}	Cell voltage range	429 mV to 431 mV
Reported average efficiency	47% (LHV)	Reported mass	451.1 t
Reported volume	821.8 m^3	–	–

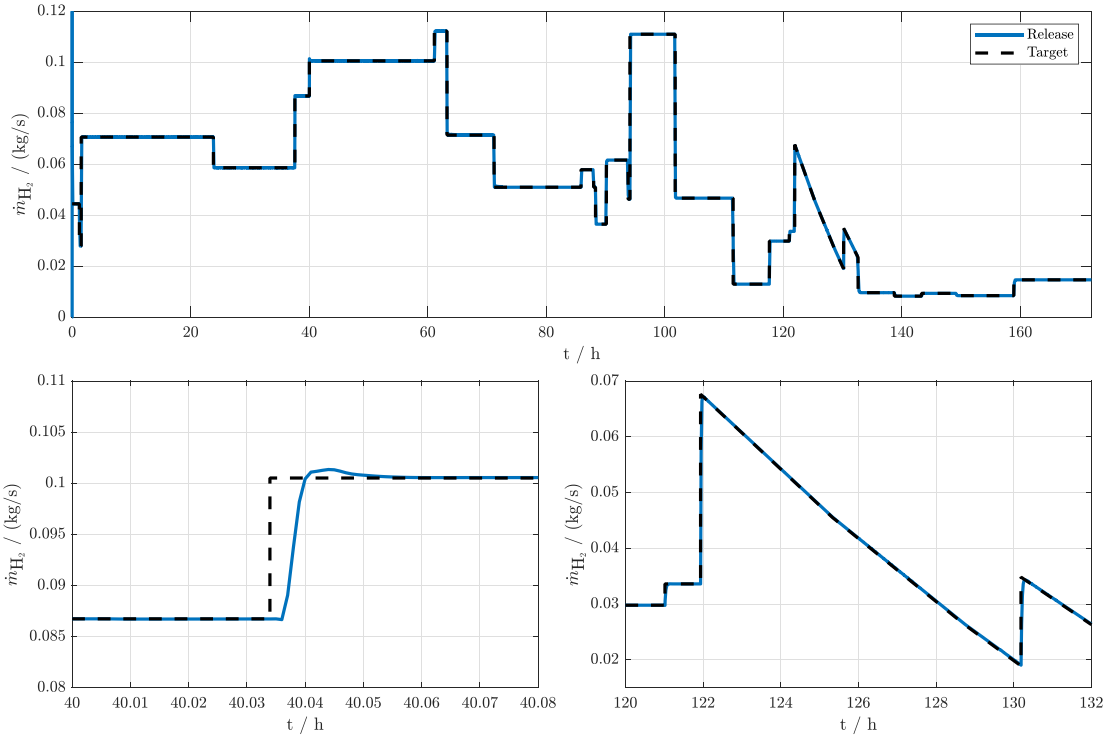

Fig. 5. Hydrogen demand (dashed line) and effective release (solid line) over time. A complete overview is provided (top panel) as well as a zoom view over step (left panel) and ramp (right panel) load transitioning.

Table 5
Simulation initial conditions and constraints on the DoH range, using NEC as the hydrogen carrier.

Variable	Value	Variable	Value
Temperature	473.15 K	Pressure	1.1 bar
Inlet mass flow rate (LOHC)	1.99 t s^{-1}	DoH_0	0.95
Minimum DoH	0.20	Maximum DoH	0.95

for temperature. Additionally, temperature changes are higher than pressure changes.

It should be highlighted that although the kinetic model is less accurate as the pressure increases due to a lack of high-pressure experimental data [31], the results obtained are still valid, because different kinetic data would simply slightly change the pressure values returned by the controller without a significant impact on the system output.

The evolution of the degree of hydrogenation is plotted in Fig. 7. As expected, the final DoH is approximately 0.20, aligning with the design choice. Steeper slopes are associated with higher load factors; the final DoH value is actually 0.1998 due to the effect of transients.

The cumulative error over time between hydrogen demand and actual release is represented in Fig. 8. At the end of the simulation the cumulative error is a positive value, associated with a hydrogen release slightly higher than designed (see the hydrogen mass supply in Table 6). Horizontal sections are associated with stationary load conditions, where the release error with respect to the demand is null. Positive slopes mean that the release is higher than the demand, while decreasing slopes mean that the hydrogen released is lower than the target value. Although limited, even the ramp-like transition in the bottom panel of Fig. 5 is actually associated with an error. More specifically, approximately 3.0 kg of hydrogen surplus are released in addition to the 117.6 kg of the hydrogen demand. As the cumulative error sign is always positive, the introduction of a hydrogen buffer could complement the already satisfactory dynamic performance of the PI controllers. The cumulative error would therefore correspond to the mass content of the vessel (maximum 11.4 kg, that is, 0.0347% of the minimum hydrogen supply). Decreasing slopes would then be associated with the emptying of the buffer, and the demand would be fully satisfied even during transients using the surplus hydrogen release stages, which would otherwise be wasted.

In general, the dynamic behavior of the LOHC system appears to be able to follow the changing load requirements. Different carriers are expected to return similar results in terms of target matching, with control variables following different trends.

3.3. LOHC system comparative design

Table 6 sums up the results of the LOHC system sizing, in terms of mass and volume of the storage subsystem for different LOHCs; the results are compared to the ammonia-based system presented in

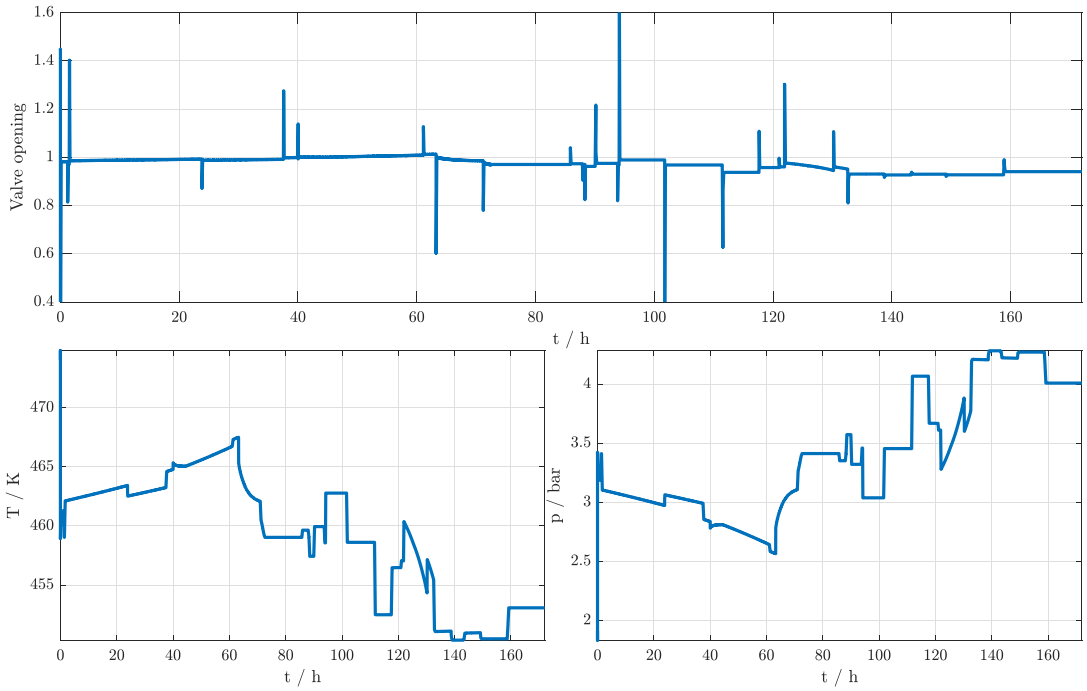

Fig. 6. Required controlled parameters trend over time to meet the hydrogen demand of Fig. 5. From top to bottom: mass flow rate control, and temperature (left) and pressure (right) secondary control.

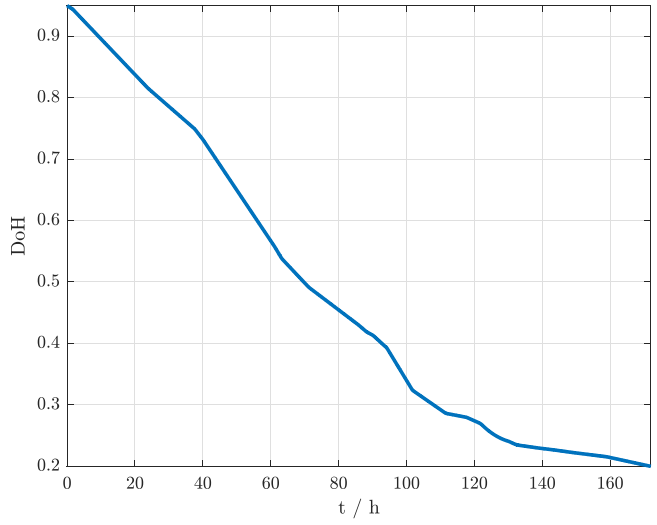

Fig. 7. Overall DoH trend over time, evaluated over the whole system (vessels and reactor).

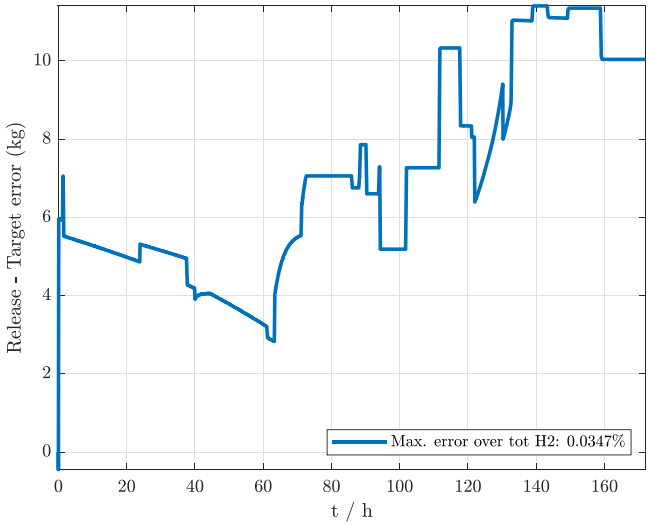

Fig. 8. Cumulative error over time between the hydrogen released and the target.

the literature [47]. The mass content is evaluated with respect to the molar mass of each carrier, while the volume of the DBT, MCH and DEC systems is evaluated with the density at 293.15 K; this value may underestimate the effective volume requirement of the operating system, if it is sized with reference to the LOHC density evaluated at the operating temperature. In the case of NEC, the volume range in Table 6 is calculated with the densities in the temperature range of 293.15 K to 473.15 K, to highlight the significant effect of temperature on LOHC density.

Matching the load profile (Fig. 1) with the sized SOFC stack returns a required chemical energy input of 1295 MWh, corresponding to the hydrogen mass indicated in Table 6 as hydrogen consumption. However, the effective mass of hydrogen stored is higher by a factor of $\mathrm{DoH}_0/\left(\mathrm{DoH}_{max}-\mathrm{DoH}_{min}\right) = 1.267$ due to the constraints on the minimum and maximum DoH, which reduce the operating DoH range to 0.75 (Table 5). For NEC systems the total mass to be stored is 748.28 t: approximately 1.8 times the mass of ammonia. Although this value is associated with an even higher hydrogen surplus of more than 26% due to the set DoH range, which could be used to some extent to provide a safety margin in case of higher power demand, a complete discharge ($\mathrm{DoH}_{min} = 0$) is unlikely to be achievable. In any case, if dehydrogenation could take place using the full DoH range (0.0 to 1.0), the required total mass would drop to 562.77 t, which would still be higher than the ammonia system by about 1.4 times. When comparing different LOHCs, the mass of NEC is the highest, which is reasonable given that the heteroatom in the aromatic ring (nitrogen inclusion)

Table 6
Mass and volume of the hydrogen storage subsystem for different LOHCs. Ammonia sizing results taken from the literature are reported in the bottom line for comparison [47].

Variable	Value	Variable	Value
Hydrogen consumption	32.87 t	Effective hydrogen stored	41.64 t
Loaded NEC and H_2 mass	748.28 t	Volume (NEC and H_2)	778.80 m^3 to 912.26 m^3
Loaded DBT and H_2 mass	690.93 t	Volume (DBT and H_2)	756.77 m^3
Loaded MCH and H_2 mass	700.66 t	Volume (MCH and H_2)	909.95 m^3
Loaded DEC and H_2 mass	594.83 t	Volume (DEC and H_2)	663.88 m^3
Ammonia mass	355.40 t	Ammonia volume	402.20 m^3

reduces the storage capacity, although it lowers the dehydrogenation temperature and reaction enthalpy [64]. The LOHC that results in the lowest mass is DEC; however, its mass is still more than 1.6 times the mass of ammonia.

Regarding the volume taken by the storage system, the NEC system requires a volume that is approximately twice that of ammonia. The MCH system is the largest because of the low density of the hydrogenated compound. The other two LOHCs result in a lower volume requirement than the ambient-temperature NEC, with again DEC providing the greatest reduction but still leading to a volume increase of approximately 1.6 times compared to ammonia.

These results are further aggravated if the different handling of the reaction products is taken into account. While ammonia produces nitrogen, which can be released in the atmosphere, unloaded LOHCs still need to be stored on board. In addition, the effective volume requirements should also take into account the reactor volume. Di Micco et al. provide a rough estimate of approximately 27.1 m^3 and 19.2 t for the heat exchanger, which should be compared to about at least a 10% volume increase over the proposed volume data in Table 6 associated with the reactor volume fraction $f_r = 0.1$ chosen in this analysis.

Finally, Fig. 9 illustrates the SOFC-LOHC thermal integration. LOHC dehydrogenation requires a heat supply to drive the endothermic reaction, which provides the main heat sink source, and to heat the LOHC entering the reactor to the operating temperature. The available SOFC waste heat is plotted against the stack current density, taking into account both the total waste heat or just the change in reaction enthalpy change; similarly, the NEC heat demand is plotted considering only the dehydrogenation reaction enthalpy change, or the total heat demand including the heat required by the LOHC to reach operating temperature conditions, as determined by the reactor temperature control. Even assuming the maximum additional heat required for temperature control ($\Delta T_{max} = T_{max} - T_{min}$, Table 3), which is actually never required for the given load profile (see the temperature panel in Fig. 6), the SOFC always provides enough waste heat to fully cover the LOHC requirement.

With specific reference to the load profile presented in Fig. 1, the SOFC system provides about 502.6 MWh of total waste heat throughout the course of the operation. Since the NEC system requires 229.20 MWh oh heat, approximately 45.6% of the SOFC waste heat must be directed to the LOHC system, at the expense of other possible cogeneration uses. The temperature control of the NEC system generates a heat demand of about 0.3 MWh, only 0.1% of the total, confirming that most of the heat demand comes from the dehydrogenation reaction enthalpy change: therefore, the curve that most closely represents the actual NEC heat demand in Fig. 9 is the one associated with just the reaction heat, as the change in the LOHC temperature is always significantly lower than the maximum possible value ΔT_{max}.

Not accounting for the negligible heat requirement of the temperature control, the heat required to drive the hydrogen release in a DBT, MCH, and DEC system is, respectively: 296.24 MWh, 309.37 MWh and 289.64 MWh. If only the reaction heat of the ammonia system is taken into account, then its heat requirement is just 139.57 MWh [65]. Although this value should be increased to account for the additional

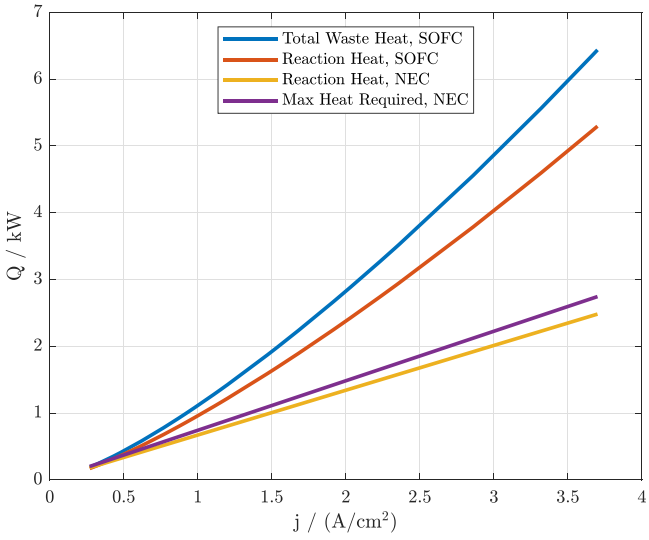

Fig. 9. SOFC waste heat, NEC reaction entalphy with respect to current density, and maximum possible heat demand. SOFC overpotential terms have been validated with [51].

heat requirements, it is still much lower than LOHCs: thus, ammonia also compares favorably to LOHCs in this regard, as its lower heat demand means that more heat is available for other purposes, possibly increasing the overall efficiency of the SOFC considered as a cogeneration unit (although this limitation is probably not as relevant for the cargo ship here considered than for a passenger ship). However, the reaction temperature of a NEC system ranges from 433.15 K to 500.15 K [53], which is significantly lower than the operating temperature of ammonia, which is approximately 663.15 K to 763.15 K [66]. In comparison, the dehydrogenation of DBT, MCH, and DEC occurs in the following temperature ranges: 563.15 K to 623.15 K [67], 453.15 K to 500.15 K [68], and 483.15 K to 563.15 K [69], respectively. While LOHC temperature ranges are lower than the operating temperature range of ammonia, even NEC systems, which are associated with the lowest temperature range, still require relatively high-quality heat.

Different carriers would return different results; however, a systematic overview of possible liquid organic hydrogen carriers reveals that the reaction enthalpy ranges from 40 kJ mol^{-1} to 70 kJ mol^{-1} and the gravimetric capacity from approximately 5.5% to 7.2% [70], which are respectively higher and lower than ammonia's properties (30.9 kJ mol^{-1} and about 17%), meaning that the advantage provided by ammonia in terms of mass and heat demand does not depend on the particular LOHC considered.

Overall, the NEC carrier has larger volume and mass constraints than any other LOHC evaluated, but with a much lower heat requirement and with the lowest reaction temperature. Conversely, the DEC system is the second next less heat-expensive carrier, and features both the lowest mass and volume constraints and moderate reaction

temperature. The MCH system, while featuring a mass content second only to that of the DEC system, is associated with the highest volume. DBT provides more intermediate properties both in terms of size and energy requirements, but features by far the highest reaction temperature. Ammonia systems are associated with both lower sizing constraints and heat requirements, but heat needs to be supplied at a higher temperature.

4. Conclusions

Current barriers to using hydrogen as fuel in maritime applications include: lack of safety requirements; low maturity of technology; onboard storage space required; high investment cost. Demonstration projects with propulsion systems using both internal combustion engines and fuel cells are ongoing. The use of compressed or liquefied hydrogen in fuel cells is a realistic option for the short-sea shipping in the medium term. The first limited demonstration applications in the ferry sector are expected this year. For ships above 5000 DWT, only two hydrogen projects were initiated before 2020, but six new projects have since begun, while for smaller vessels, twelve projects were initiated before 2020, and five since, demonstrating a shift toward hydrogen projects focusing on larger ships. However, ammonia is expected to be the best hydrogen storage option, especially for large-scale applications [3].

This paper provides both a feasibility study of LOHC storage solutions for cargo ships and a comparison between ammonia- and LOHC-based storage. The results available in the literature for an ammonia storage SOFC powertrain were chosen as Ref. [47]; the feasibility of the system was evaluated in terms of the dynamic performance with respect to the changing load.

The sizing and heat management aspects for four LOHC systems (DBT, MCH, DEC, and NEC) are presented, the latter being used to discuss the dynamic response. Dynamic simulations of the ship load reveal that LOHC systems can meet the changing target requirements, thanks to the primary LOHC flow rate control and secondary additional temperature and pressure control systems. The inlet mass valve opening goes through an initial fast variation due to the step increase or decrease, while temperature and pressure variations mostly deal with keeping the set-point release over time. Going from step to ramp load variations further alleviates the errors during transients, which are already limited. Intermediate hydrogen buffers could potentially remove any error, albeit at the cost of further volume constraints.

Despite the good dynamic response of the system, the LOHC volume and mass required to store the needed hydrogen are significantly higher than in the case of ammonia. DEC features the lowest size, with NEC the highest mass, and MCH the highest volume. On the other hand, ammonia systems are also associated with a lower dehydrogenation heat, meaning that SOFC systems operating as cogeneration units are less impacted by thermal coupling with the storage system. NEC results in the lowest energy requirement among LOHCs, while MCH has the highest. Reaction temperature ranges are lower for LOHC systems than ammonia's; however, LOHCs still require high-quality heat. Life Cycle Analysis (LCA) tools may disclose other benefits for LOHC systems, especially when accounting for the possibility to re-use the existing infrastructure for long-distance transport. However, technical feasibility would still be hindered by the low energy density.

Overall, while LOHCs are capable of meeting the load demand, these hydrogen carriers result in heavier and larger storage systems compared to ammonia and also absorb more heat; therefore, LOHCs are probably not the best option to store hydrogen for maritime applications.

Nomenclature

D	Diffusion coefficient ($m^2\ s^{-1}$)
E_{H_2}	Hydrogen chemical energy (MWh)
E_a	Activation energy ($J\ mol^{-1}$)
F	Faraday constant ($9.6485 \times 10^4\ C\ mol^{-1}$)
I	Current (A)
j	Current density ($A\ m^{-2}$)
k	Frequency factor (s^{-1})
m	Mass (kg)
$\dot{m}$	Mass flow rate ($kg\ s^{-1}$)
M	Molar mass ($g\ mol^{-1}$)
n_{cell}	Number of cells in the stack
P	Power (MW)
p	Pressure (bar)
R	Universal gas constant ($8.3145\ J\ mol^{-1}\ K^{-1}$)
T	Temperature (K)
t	Time (h)
U_f	Fuel utilization factor (%)
V	Voltage (V)
w	Maximum LOHC hydrogen gravimetric capacity (%)
z	Moles of electrons involved in the fuel cell reaction
Greek letters	
δ	Thickness (m)
γ	Exponential factor ($A\ m^{-2}$)
η	Efficiency (%)
σ	Electrical conductivity ($S\ m^{-1}$)
Subscripts	
a	Anode
c	Cathode
el	Electrolyte
Acronyms	
DBT	DiBenzylToluene
DEC	Decaline
DoH	Degree of Hydrogenation
DWT	Deadweight Tonnage
FC	Fuel Cell
GHG	Greenhouse gas
HHV	Higher Heating Value ($MJ\ kg^{-1}$)
IMO	International Maritime Organization
LCA	Life Cycle Assessment
LHV	Lower Heating Value ($MJ\ kg^{-1}$)
LOHC	Liquid Organic Hydrogen Carrier
MCH	Methylcyclohexane
NEC	N-EthylCarbazole
PEMFC	Proton Exchange Membrane Fuel Cell
PI	Proportional–Integral
SOFC	Solid Oxide Fuel Cell
TOL	Toluene
TPB	Triple Phase Boundary

CRediT authorship contribution statement

Marco Gambini: Visualization, Validation. **Federica Guarnaccia:** Writing – review & editing, Writing – original draft, Visualization, Validation, Software, Methodology, Conceptualization. **Michele Manno:** Writing – review & editing, Visualization, Validation, Supervision, Methodology, Conceptualization. **Michela Vellini:** Visualization, Validation.

Declaration of competing interest

The authors declare that they have no known competing financial interests or personal relationships that could have appeared to influence the work reported in this paper.

References

[1] European Commission. Reducing emissions from the shipping sector. 2024, URL https://climate.ec.europa.eu/eu-action/transport/reducing-emissions-shipping-sector_en.

[2] Marine Environment Protection Committee. Resolution mepc.377(80): 2023 imo strategy on reduction of GHG emissions from ships. 2023, URL https://wwwcdn.imo.org/localresources/en/MediaCentre/PressBriefings/Documents/Clean%20version%20of%20Annex%201.pdf.

[3] Hammer LS, Eide MS, Leisner M, Longva T, Endresen Ø, Rivedal NH, Ovrum E, Sekkesaeter Ø, Nyset H, Nyhus E, Mjelde A, Walenkiewicz J, Helgesen H, Simonsen EB, Jaeouk S, Adams S, Schäfer J. Maritime forecast to 2050. Technical report, DNV; 2021, URL https://www.dnv.com/maritime/publications/maritime-forecast-2023/.

[4] Pashchenko D. Ammonia fired gas turbines: Recent advances and future perspectives. Energy 2024;290:130275. http://dx.doi.org/10.1016/j.energy.2024.130275.

[5] Afif A, Radenahmad N, Cheok Q, Shams S, Kim JH, Azad AK. Ammonia-fed fuel cells: a comprehensive review. Renew Sustain Energy Rev 2016;60:822–35. http://dx.doi.org/10.1016/j.rser.2016.01.120.

[6] Laursen R, Patel H, Dowling M, Sofiadi D, Ji D, Király R, Pang E. Potential of hydrogen as fuel for shipping. Technical report, European Maritime Safety Agency; 2023, URL https://www.emsa.europa.eu/publications/item/5062-potential-of-hydrogen-as-fuel-for-shipping.html.

[7] Abe A, Nakamura M, Sato I, Uetani H, Fujitani T. Studies of the large-scale sea transportation of liquid hydrogen. Int J Hydrog Energy 1998;23(2):115–21. http://dx.doi.org/10.1016/S0360-3199(97)00032-3.

[8] Ustolin F, Campari A, Taccani R. An extensive review of liquid hydrogen in transportation with focus on the maritime sector. J Mar Sci Eng 2022;10(9):1222. http://dx.doi.org/10.3390/jmse10091222.

[9] Kolodziejski M. Review of hydrogen-based propulsion systems in the maritime sector. Arch Thermodyn 2023;44(4):335–80. http://dx.doi.org/10.24425/ather.2023.149728.

[10] Kolodziejski M, Michalska-Pozoga I. Battery energy storage systems in ships' hybrid/electric propulsion systems. Energies 2023;16(3):1122. http://dx.doi.org/10.3390/en16031122.

[11] MAN Truck & Bus. MAN engines: The first dual fuel hydrogen engines in use on a work boat. 2022, URL https://press.mantruckandbus.com/corporate/man-engines-the-first-dual-fuel-hydrogen-engines-in-use-on-a-work-boat/.

[12] Windcat Workboats. Elevation series. 2024, URL https://www.windcatworkboats.com/csov-fleet/.

[13] Port of Antwerp-Bruges and CMB.TECH Hydrotug 1 hydrogen-powered tugboat ready for operation; BeHydro V12 dual-fuel medium-speed engines. 2023, URL https://www.greencarcongress.com/2023/12/20231213-hydrotug.html.

[14] Edda Wind. Edda breeze. 2023, URL https://eddawind.com/vessels/edda-breeze/.

[15] Yachting World. Energy Observer: From ocean racer to tech wonder. 2021, URL https://www.yachtingworld.com/extraordinary-boats/energy-observer-from-ocean-racer-to-tech-wonder-132195.

[16] Nagy-McKenna C. Meet the Energy Observer, the World's First Hydrogen-powered Boat and Trailblazing Energy Laboratory. 2023, URL https://www.enerdynamics.com/Energy-Currents_Blog/Meet-the-Energy-Observer-the-Worlds-First-Hydrogen-powered-Boat-and-Trailblazing-Energy-Laboratory.aspx.

[17] Prevljak NH. Energy Observer unveils zero-emission, LH2-powered cargo ship concept. 2022, URL https://www.offshore-energy.biz/energy-observer-unveils-lh2-powered-cargo-ship-concept/.

[18] Gable N. BAE Systems provides propulsion system for first U.S. marine vessel with zero-emission fuel cell technology. 2021, URL https://bit.ly/3KuMK3c.

[19] All American Marine. Hydrogen fuel cell passenger ferry for SWITCH maritime. 2023, URL https://www.allamericanmarine.com/vessels-gallery/sea-change-hydrogen/.

[20] Corvus Energy. MF HYDRA. 2023, URL https://corvusenergy.com/projects/mf-hydra/.

[21] Bahtić F. PowerCell to provide hydrogen solutions for two Norwegian state ferries. 2023, URL https://www.offshore-energy.biz/powercell-to-provide-hydrogen-solutions-for-two-norwegian-state-ferries/.

[22] Minutillo M, Cigolotti V, Di Ilio G, Bionda A, Boonen E-J, Wannemacher T. Hydrogen-based technologies in maritime sector: technical analysis and prospective. In: E3S web of conferences. Vol. 334, 2022, p. 06011. http://dx.doi.org/10.1051/e3sconf/202233406011.

[23] Pashchenko D. Green hydrogen as a power plant fuel: What is energy efficiency from production to utilization? Renew Energy 2024;223:120033. http://dx.doi.org/10.1016/j.renene.2024.120033.

[24] Di Micco S, Mastropasqua L, Cigolotti V, Minutillo M, Brouwer J. A framework for the replacement analysis of a hydrogen-based polymer electrolyte membrane fuel cell technology on board ships: A step towards decarbonization in the maritime sector. Energy Convers Manage 2022;267:115893. http://dx.doi.org/10.1016/j.enconman.2022.115893.

[25] Perna A, Jannelli E, Di Micco S, Romano F, Minutillo M. Designing, sizing and economic feasibility of a green hydrogen supply chain for maritime transportation. Energy Convers Manage 2023;278:116702. http://dx.doi.org/10.1016/j.enconman.2023.116702.

[26] Watanabe MD, Cherubini F, Tisserant A, Cavalett O. Drop-in and hydrogen-based biofuels for maritime transport: Country-based assessment of climate change impacts in Europe up to 2050. Energy Convers Manage 2022;273:116403. http://dx.doi.org/10.1016/j.enconman.2022.116403.

[27] dos Santos VA, Pereira da Silva P, Serrano LMV. The maritime sector and its problematic decarbonization: A systematic review of the contribution of alternative fuels. Energies 2022;15(10):3571. http://dx.doi.org/10.3390/en15103571.

[28] American Bureau of Shipping. Guide for gas and other low-flashpoint fuel ready vessels july 2020. 2020, URL https://safety4sea.com/wp-content/uploads/2020/09/ABS-gas-and-other-low-flashpoint-fuel-ready-vessels-2020_09.pdf.

[29] Panić I, Cuculić A, Ćelić J. Color-coded hydrogen: Production and storage in maritime sector. J Mar Sci Eng 2022;10(12):1995. http://dx.doi.org/10.3390/jmse10121995.

[30] Štádlerová Š, Schütz P. Designing the Hydrogen Supply Chain for Maritime transportation in Norway. In: Computational logistics. Springer International Publishing; 2021, p. 36–50. http://dx.doi.org/10.1007/978-3-030-87672-2_3.

[31] Gambini M, Di Vona ML, Guarnaccia F, Manno M, Vellini M. Liquid organic hydrogen carriers: Development of a thermodynamic and kinetic model for the assessment of hydrogenation and dehydrogenation processes. Int J Hydrog Energy 2022;47(65):28034–45. http://dx.doi.org/10.1016/j.ijhydene.2022.06.120.

[32] Niermann M, Drünert S, Kaltschmitt M, Bonhoff K. Liquid organic hydrogen carriers (LOHCs) – techno-economic analysis of LOHCs in a defined process chain. Energy Environ Sci 2019;12:290–307. http://dx.doi.org/10.1039/C8EE02700E.

[33] Preuster P, Papp C, Wasserscheid P. Liquid organic hydrogen carriers (LOHCs): Toward a hydrogen-free hydrogen economy. Acc Chem Res 2017;50(1):74–85. http://dx.doi.org/10.1021/acs.accounts.6b00474.

[34] Chiefari J, Hornung C. Mobile hydrogen reformers as a novel approach to decarbonise the transport sector. Curr Opin Chem Eng 2021;34:100756. http://dx.doi.org/10.1016/j.coche.2021.100756.

[35] Fikrt A, Brehmer R, Milella V-O, Müller K, Bösmann A, Preuster P, Alt N, Schlücker E, Wasserscheid P, Arlt W. Dynamic power supply by hydrogen bound to a liquid organic hydrogen carrier. Appl Energy 2017;194:1–8. http://dx.doi.org/10.1016/j.apenergy.2017.02.070.

[36] Bollmann J, Mitländer K, Beck D, Schühle P, Bauer F, Zigan L, Wasserscheid P, Will S. Burner-heated dehydrogenation of a liquid organic hydrogen carrier (LOHC) system. Int J Hydrog Energy 2023;48(77):30039–56. http://dx.doi.org/10.1016/j.ijhydene.2023.04.062.

[37] Aakko-Saksa PT, Cook C, Kiviaho J, Repo T. Liquid organic hydrogen carriers for transportation and storing of renewable energy – Review and discussion. J Power Sources 2018;396:803–23. http://dx.doi.org/10.1016/j.jpowsour.2018.04.011.

[38] Pashchenko D. Liquid organic hydrogen carriers (LOHCs) in the thermochemical waste heat recuperation systems: The energy and mass balances. Int J Hydrog Energy 2022;47(67):28721–9. http://dx.doi.org/10.1016/j.ijhydene.2022.06.208.

[39] Spatolisano E, Restelli F, Matichecchia A, Pellegrini LA, de Angelis AR, Cattaneo S, Roccaro E. Assessing opportunities and weaknesses of green hydrogen transport via LOHC through a detailed techno-economic analysis. Int J Hydrog Energy 2024;52:703–17. http://dx.doi.org/10.1016/j.ijhydene.2023.08.040.

[40] Fragiacomo P, Piraino F, Genovese M, Corigliano O, De Lorenzo G. Experimental activities on a hydrogen-powered solid oxide fuel cell system and guidelines for its implementation in aviation and maritime sectors. Energies 2023;16(15):5671. http://dx.doi.org/10.3390/en16155671.

[41] Yang Y, Wu Z, Li R, Wang H, Ren J, Li B, Yang F, Zhang Z. Review on the thermal neutrality of application-oriented liquid organic hydrogen carrier for hydrogen energy storage and delivery. Res Eng 2023;19:101394. http://dx.doi.org/10.1016/j.rineng.2023.101394.

[42] Preuster P, Fang Q, Peters R, Deja R, Nguyen VN, Blum L, Stolten D, Wasserscheid P. Solid oxide fuel cell operating on liquid organic hydrogen carrier-based hydrogen – making full use of heat integration potentials. Int J Hydrog Energy 2018;43(3):1758–68. http://dx.doi.org/10.1016/j.ijhydene.2017.11.054.

[43] Preuster P, Fang Q, Peters R, Deja R, Nguyen VN, Blum L, Stolten D, Wasserscheid P. A solid oxide fuel cell operating on liquid organic hydrogen carrier-based hydrogen – A kinetic model of the hydrogen release unit and system performance. Int J Hydrog Energy 2019;44(26):13794–806. http://dx.doi.org/10.1016/j.ijhydene.2019.03.220.

[44] Singh D, Pedersen E. A review of waste heat recovery technologies for maritime applications. Energy Convers Manage 2016;111:315–28. http://dx.doi.org/10.1016/j.enconman.2015.12.073.

[45] Micoli L, Russo R, Coppola T, Pietra A. Performance Assessment of the Heat Recovery System of a 12 MW SOFC-Based Generator on Board a Cruise Ship through a 0D Model. Energies 2023;16:3334. http://dx.doi.org/10.3390/en16083334.

[46] Ouyang T, Zhao Z, Lu J, Su Z, Li J, Huang H. Waste heat cascade utilisation of solid oxide fuel cell for marine applications. J Clean Prod 2020;275:124133. http://dx.doi.org/10.1016/j.jclepro.2020.124133.

[47] Di Micco S, Cigolotti V, Mastropasqua L, Brouwer J, Minutillo M. Ammonia-powered ships: Concept design and feasibility assessment of powertrain systems for a sustainable approach in maritime industry. Energy Convers Manage: X 2024;22:100539. http://dx.doi.org/10.1016/j.ecmx.2024.100539.
[48] Kiermaier S, Lehmann D, Bösmann A, Wasserscheid P. Dehydrogenation of perhydro-N-ethylcarbazole under reduced total pressure. Int J Hydrog Energy 2021;46(29):15660–70. http://dx.doi.org/10.1016/j.ijhydene.2021.02.128.
[49] Aijjou, Raihani, Bahatti. Study on container ship energy consumption. In: WIT transactions on ecology and the environment. energy and sustainability VIII. Vol. 237, 2019, p. 25–36. http://dx.doi.org/10.2495/ESUS190031.
[50] Hafsia A, Bariza Z, Djamel H, Hocine BM, Andreadis GM, Soumia A. SOFC fuel cell heat production: Analysis. Energy Procedia 2011;6:643–50. http://dx.doi.org/10.1016/j.egypro.2011.05.074.
[51] Ranjbar F, Chitsaz A, Mahmoudi S, Khalilarya S, Rosen MA. Energy and exergy assessments of a novel trigeneration system based on a solid oxide fuel cell. Energy Convers Manage 2014;87:318–27. http://dx.doi.org/10.1016/j.enconman.2014.07.014.
[52] Yang, Chen, Wang, Peng, Wang. Electrochemical analysis of an anode-supported SOFC. Int J Electrochem Sci 2013;8(2):2330–44. http://dx.doi.org/10.1016/S1452-3981(23)14312-4.
[53] Gambini M, Guarnaccia F, Manno M, Vellini M. Flow rate control in a plug-flow reactor for liquid organic hydrogen carriers dehydrogenation. Int J Hydrog Energy 2024;62:375–88. http://dx.doi.org/10.1016/j.ijhydene.2024.03.082.
[54] Brigljević B, Byun M, Lim H. Design, economic evaluation, and market uncertainty analysis of LOHC-based, CO_2 free, hydrogen delivery systems. Appl Energy 2020;274:115314. http://dx.doi.org/10.1016/j.apenergy.2020.115314.
[55] Wan C, An Y, Xu G, Kong W. Study of catalytic hydrogenation of N-ethylcarbazole over ruthenium catalyst. Int J Hydrog Energy 2012;37(17):13092–6. http://dx.doi.org/10.1016/j.ijhydene.2012.04.123.
[56] Kim S, Chen J, Cheng T, Gindulyte A, He J, He S, Li Q, Shoemaker BA, Thiessen PA, Yu B, Zaslavsky L, Zhang J, Bolton EE. PubChem 2023 update. Nucl Acids Res 2022;51(D1):D1373–80. http://dx.doi.org/10.1093/nar/gkac956.
[57] Hydrogen supply and transportation using Liquid Organic Hydrogen Carriers (HYSTOC). 2018, http://dx.doi.org/10.3030/779694, Horizon 2020. Grant agreement ID: 779694.
[58] Rao PC, Yoon M. Potential liquid-organic hydrogen carrier (LOHC) systems: A review on recent progress. Energies 2020;13(22):6040. http://dx.doi.org/10.3390/en13226040.
[59] Gambini M, Guarnaccia F, Manno M, Vellini M. Thermal design and heat transfer optimisation of a liquid organic hydrogen carrier batch reactor for hydrogen storage. Int J Hydrog Energy 2023;48(96):37625–36. http://dx.doi.org/10.1016/j.ijhydene.2023.08.200.
[60] Gambini M, Guarnaccia F, Manno M, Vellini M. Ragone plots of material-based hydrogen storage systems. J Energy Storage 2024;76:109815. http://dx.doi.org/10.1016/j.est.2023.109815.
[61] Bourane A, Elanany M, Pham TV, Katikaneni SP. An overview of organic liquid phase hydrogen carriers. Int J Hydrog Energy 2016;41(48):23075–91. http://dx.doi.org/10.1016/j.ijhydene.2016.07.167.
[62] Brinks H. Ammonia-fuelled engines for carbon free shipping. 2021, URL https://www.dnv.com/research/review-2021/featured-projects/ammonia-fuelled-engines/. AEngine project.
[63] Dincer I, Zamfirescu C. Chapter 4 - Hydrogen and Fuel Cell Systems. In: Dincer I, Zamfirescu C, editors. Advanced Power Generation Systems. Boston: Elsevier; 2014, p. 143–98. http://dx.doi.org/10.1016/B978-0-12-383860-5.00004-3.
[64] Le T-H, Tran N, Lee H-J. Development of Liquid Organic Hydrogen Carriers for Hydrogen Storage and Transport. Int J Mol Sci 2024;25(2):1359. http://dx.doi.org/10.3390/ijms25021359.
[65] Ristig S, Poschmann M, Folke J, Gómez-Cápiro O, Chen Z, Sanchez-Bastardo N, Schlögl R, Heumann S, Ruland H. Ammonia Decomposition in the Process Chain for a Renewable Hydrogen Supply. Chem Ing Tech 2022;94(10):1413–25. http://dx.doi.org/10.1002/cite.202200003.
[66] Moszczyńska J, Liu X, Wiśniewski M. Green Hydrogen Production through Ammonia Decomposition Using Non-Thermal Plasma. Int J Mol Sci 2023;24(18):14397. http://dx.doi.org/10.3390/ijms241814397.
[67] Park S, Naseem M, Lee S. Experimental Assessment of Perhydro-Dibenzyltoluene Dehydrogenation Reaction Kinetics in a Continuous Flow System for Stable Hydrogen Supply. Materials 2021;14:7613. http://dx.doi.org/10.3390/ma14247613.
[68] Tsai Y, Cai J, Pan Y, Jiang J. Explosion risk assessment of a liquid organic hydrogen carrier system by using toluene–methylcyclohexane on varying hydrogen storage scenarios. J Loss Prev Process Ind 2023;86:105206. http://dx.doi.org/10.1016/j.jlp.2023.105206.
[69] Hodoshima S, Takaiwa S, Shono A, Satoh K, Saito Y. Hydrogen storage by decalin/naphthalene pair and hydrogen supply to fuel cells by use of superheated liquid-film-type catalysis. Appl Catal A: Gen 2005;283(1):235–42. http://dx.doi.org/10.1016/j.apcata.2005.01.010.
[70] Harb H, Elliott SN, Ward L, Foster IT, Klippenstein SJ, Curtiss LA, Assary RS. Uncovering novel liquid organic hydrogen carriers: a systematic exploration of chemical compound space using cheminformatics and quantum chemical methods. Digit Discov 2023;2. http://dx.doi.org/10.1039/D3DD00123G.